UNIVERSITY OF CALIFORNIA, SAN DIEGO

Understanding the Role of the Microtubule Cytoskeleton in Synapse Formation and Maintenance

A Thesis submitted in partial satisfaction of the requirements for the degree

Master of Science

in

Biology

by

Karina Jean Kono

Committee in charge:

Yishi Jin, Chair
Amy Pasquinelli, Co-Chair
Ella Tour

2017

The Thesis of Karina Jean Kono is approved and it is acceptable in quality and form for publication on microfilm and electronically:

_____

_____

Co-Chair

_____

Chair

University of California, San Diego

2017

DEDICATION

For my mother, father, and brother because I could not have asked for a better family to be born into.

And for Stephanie Helene who always supports each and every endeavor I undertake and without whom I would have never seen my work through to the finish.

Special thanks to CL, JD, SW, CP, and JR for their friendship that carried me through my time here.

TABLE OF CONTENTS

LIST OF TABLES

LIST OF FIGURES

ACKNOWLEDGMENTS

I would like to thank the members of the Jin and Chisholm lab for all the help in troubleshooting experiments and guidance in presentations, posters, and writing.

Of considerable note:

Dr. Naina Kurup for mentoring me through my undergraduate and graduate research, all the while maintaining patience as I learned basic techniques. For teaching me all the skills I now have in scientific communication and bench work. And for the constant positive feedback that kept my morale high when my project seemed too complicated or I felt I wasn't enough to finish.
Dr. Katherine McCulloch for all the advice in two-point mapping techniques and for the great recommendations ranging from science-fiction literature, television, and film to Roman history podcasts and coffee shops.
Dr. Salvatore Cherra for his tech support skills and patience with my many and varied questions about life in academia and beyond.

And a special thanks to Dr. Yishi Jin for taking the risk of giving me a position in her lab as a fourth-year student with no research experience and poor communication skills. Her advice and guidance have helped me to grow and push myself to continue learning, taking on projects I would have considered out of my reach just two years ago.

ABSTRACT OF THE THESIS

Understanding the Role of the Microtubule Cytoskeleton in Synapse Formation and Maintenance

by

Karina Jean Kono

Master of Science in Biology

University of California, San Diego, 2017

Professor Yishi Jin, Chair

Professor Amy Pasquinelli, Co-Chair

Microtubules are polymeric filaments that cross the cell made up of alpha- and beta- tubulin heterodimers. These structures exist in a dynamic state in which they switch between phases of polymerization and de-polymerization; this cycling is termed dynamic instability. Dynamic instability is under tight control by microtubule-associated proteins that can either promote stabilization and growth, or destabilization and decay.

Dynamic microtubules are incredibly important for neurons to function correctly and for the normal development of the nervous system. Many neural disorders can be characterized by disruption to the microtubule network by either altering tubulin or the proteins that regulate microtubules. Here, we use an alpha-tubulin mutant in *C. elegans* that causes synaptic defects in a screen for microtubule associated proteins. The combination of the alpha-tubulin mutation with a loss of DLK-1 causes enhanced synaptic defects. A forward genetic screen in our lab in the double mutant background produced a mutant that ameliorates the deficits. Here, I present how I mapped this mutation to the beta-tubulin gene *tbb-2*. I also describe a screen I performed to look for suppressors of the *tba-1* single mutant synaptic defects.

INTRODUCTION

Microtubule dynamics are essential for normal neuronal functions

The nervous system processes all the various stimuli that we experience and sends signals for an appropriate response. It is made up of many neurons that have formed connections to specific targets in organized patterns. Tightly regulated development and careful maintenance allow the nervous system to maintain its complexity and function.

An immature neuron must extend a process toward its target, establish a physical connection with that target, and also be able to recognize connections made onto itself. As the sub-cellular level, these processes are dependent on properly regulated changes to the cytoskeleton (Chakraborti, Natarajan, Curiel, Janke, & Liu, 2016; Conde & Cáceres, 2009).

Microtubules are a large component of the cytoskeleton. A single microtubule is a tubular protein-complex formed from bundled protofilaments that are in turn made up of heterodimer subunits of alpha- and beta-tubulin. Rather than remain at a constant length, microtubules switch between periods of growth and shrinkage, termed dynamic instability (Conde & Cáceres, 2009).

Dynamic instability is tightly controlled by microtubule-associated proteins. These proteins bind to the microtubule and can stabilize them, promoting growth. Doublecortin is one such stabilizing protein that binds microtubules and allows

them to bundle (Horesh et al., 1999). Other microtubule-associated proteins physically shear apart protofilaments and promote depolymerization. Katanin, for example, puts physical strain on the microtubule lattice that causes the subunits to break away from each other (Hartman & Vale, 1999). The motor proteins dynein and kinesin are known to walk along microtubules, tugging cargo-filled vesicles to their targets. Recent investigation has shown that kinesins can weakly bind microtubules at their cargo-binding domain and this double-binding organizes microtubule growth direction (Molodtsov et al., 2016).

The growth and rapid disassembly allow cells to “feel” out their environment. In the growth cone of an extending axon, many dynamic microtubules are helping the cell to probe the area. Once a cue is sensed, microtubules growing toward that cue are captured and stabilized. The other microtubules are allowed to retract and the axon grows towards the cue (Gordon-weeks, 2003). In synapse formation, special microtubule structures are formed called synaptic boutons. These looped microtubule structures are essential to establish a synapse (Conde & Cáceres, 2009).

Microtubule dynamics become disrupted in neural dysfunction and disease

Thus, disruption of microtubule dynamics leads to disruption in normal neuronal processes. For example, aberrant expression of microtubule-associated

proteins that stabilize microtubules resulted in irregular growth of synaptic boutons (Roos, Hummel, Ng, Klämbt, & Davis, 2000; Ruiz-canada et al., 2004).

In fact, many neuronal diseases have been linked to mutations in microtubule and microtubule-associated protein genes (Baird & Bennett, 2013).

Lissencephaly is a condition in which the brain does not develop its characteristic folds and valleys and is instead smooth. The disease is linked to mutations in alpha-tubulin, beta-tubulin, and the microtubule stabilizing protein doublecortin (Baumbach et al., 2017; Horesh et al., 1999). A characteristic of Parkinson's disease is the appearance of Lewy bodies in neurons that have been found to contain tubulin fragments. Additionally, the classic Parkinson's gene, PINK1, was recently described to also affect microtubule stability and not just mitochondria degradation(Cartelli & Cappelletti, 2016; Pellegrini, Wetzel, Grannó, Heaton, & Harvey, 2017).

Therefore, it is important that we explore key-players in microtubule regulation to better understand how their disruption contributes to disease.

C. elegans **as a model organism for neurobiological study**

C. elegans is a nematode found ubiquitously throughout the world. These microscopic animals provide a powerful tool for study. Their translucent bodies facilitate imaging with fluorescent-tagged proteins that gives us a lot of information about protein localization and cellular structures. They are also self-

fertilizing hermaphrodites which makes establishing homozygous mutant strains that are clones of the original very easy. Because they have the ability to mate with males (which occur spontaneously in a population at low rates or may arise with heat shock treatment in a lab), we can also establish new strains by setting up genetic crosses.

The *C. elegans* genome is also relatively small. All genetic information is contained on six chromosomes, relatively the same size. Despite its smaller size, worms contain about 20,000 genes with many homologues shared with mammal species, making them a relevant organism for study. Not only that, but the entire worm genomes has been sequenced and many genes mapped throughout (Brenner, 1974).

Due to their large brood size and ease of mutagenesis to their germ line, these animals are a great organism to use in genetic screens that identify genes in desired pathways.

A previous forward-genetic screen in *C. elegans* produced many mutants that exhibited various synaptic defects when visualized under the compound scope. One particular mutation, *ju89*, is a gain-of-function mutation in the C-terminal domain of alpha-tubulin, TBA-1. This mutation changes a conserved glycine to arginine (G414R) and, because it occurs at the external face of the microtubule, interferes with microtubule associated protein binding ability (Figure 0.1 A). This mutation can be identified by its behavioral phenotype. *C. elegans* alternately contract and relax body opposing body wall muscles which gives the

animal its characteristic wave-like movement pattern. *tba-1(ju89)* mutants however, are unable to properly coordinate this action and move more slowly and in a straight line (Figrue 0.1 B,D). When viewed on the compound scope, we can see that the mutation also alters synapse morphology (Figure 0.1 C,E). Animals carrying this mutation have a reduced number of synapses. There are also many abnormalities in the size and spacing of synapses along the dorsal nerve cord and a variety of commissure outgrowth defects (Baran et al., 2010).

Previously in our lab, *tba-1(ju89)* was used to put stress on the microtubule cytoskeleton in a DLK-1 null background, *dlk-1(tm4024)*. The resulting double mutant, *tba-1(ju89) dlk-1(tm4024)*, is severely uncoordinated, nearly to the point of paralysis. This is due to a developmental defect in these animals in which they fail to undergo a circuit rewiring program, termed DD-remodeling, and therefore a whole subset of neurons do not connect to the proper targets (Kurup, Yan, Goncharov, & Jin, 2015; Petersen et al., 2011).

I present, first, how I mapped a suppressor of the *tba-1(ju89) dlk-1(tm4024)* remodeling defect to the beta-tubulin gene *tbb-2*. I found that the new allele is gain-of-function and suppresses both the remodeling defects of the double mutant and the comparatively milder synaptic defects of *tba-1(ju89)*.

Next, I discuss a screen I performed for suppressors of *tba-1(ju89).* Dr. Naina Kurup, a member of our lab, created the strain CZ23343 [*tba-1(ju89); juIs137; juSi292*] that contains two extra copies of full-length, genomic *tba-1(ju89)* inserted on chromosome IV. I characterize the insertion by crossing it into

a variety of genetic backgrounds and noting the effects on synaptic and behavior phenotypes. We used both *tba-1(ju89)* and *tba-1(ju89); juSi292* in our screen and found one suppressor that significantly restores movement and synapse morphology.

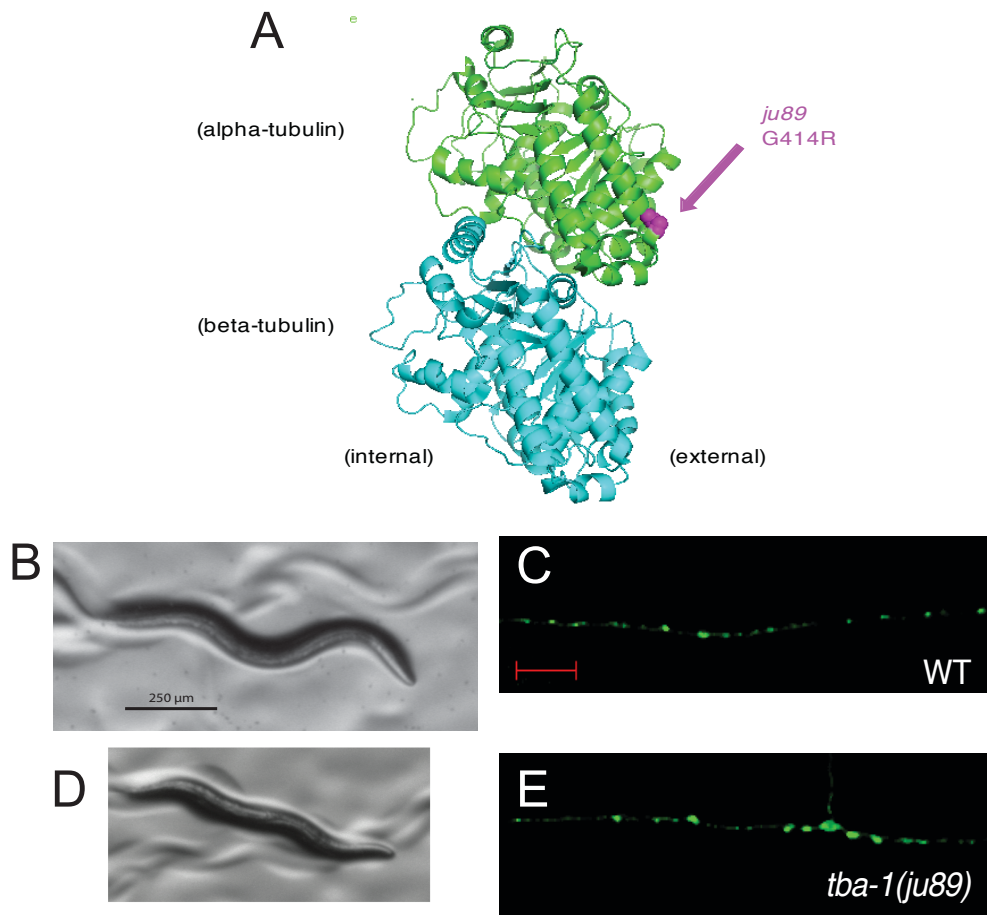

Figure 0.1: tba-1(ju89) causes synaptic and behavioral defects I **A** Heterodimer crystal structure of alpha (green) and beta-tubulin (blue). ju89 location and amino acid change annotated in purple. **B,D** Behavior of wild-type (B) and tba-1(ju89) (D) animals. **C, E** P_{flp-13}-SNB-1::GFP in wild-type (C) and tba-1(ju89) (E) animals. Synaptic defects in tba-1(ju89) animals can be seen by the gaps in-between puncta and irregular size of puncta. Scale bar (red) represents 10 µm.

.

CHAPTER 1: A gain-of-function mutation in *tbb-2* suppresses DD-remodeling defects in *tba-1(ju89) dlk-1(tm4024)*

Background

C. elegans contain a subset of GABAergic neurons, DD neurons, that undergo circuit re-wiring in the L1 stage (Petersen et al., 2011; WHITE, ALBERTSON, & ANNESS, 1978). When the DD neurons are born, they first synapse onto ventral body wall muscle. By the end of L2, these synapses have been eliminated and re-established onto dorsal body wall muscle, all without changing neuron morphology (Figure 1.1). Dynamic microtubules are known to play an essential role in this process (Kurup et al., 2015).

Previous work from our lab found that the gain-of-function mutation *ju89* in combination with the loss of a kinase, DLK-1, involved in neural development enhanced synaptic defects. These double mutants, referred to as *tba-1(ju89) dlk-1(tm4024)*, fail to undergo DD remodeling; synapses in DD-neurons are retained along the ventral nerve cord and synaptic vesicles aggregated in the commissures (Figure 1.2). Analysis found that the double-mutant had longer, more stable microtubules (Kurup et al., 2015). The double mutant animal is also characterized by its severely uncoordinated movement: they are nearly paralyzed by adult stage and are unable to initiate backwards movement in response to tapping on the head.

A suppressor screen in this double mutant background yielded several suppressing mutations that have been mapped to different microtubule genes. Eight were intragenic mutations of *tba-1*, seven were mapped to the motor proteins dynein and kinesin, and one was in a tau-tubulin kinase (Kurup, Yan, Kono, & Jin, 2017). Here, I mapped one unknown mutation to the beta-tubulin gene, *tbb-2*.

Materials and methods

Strain maintenance and genetic crosses

All strains were maintained on NGM plates as described (Brenner, 1974). Plates were kept on the benchtop at 22°C. Strains received from outside sources were outcrossed to N2 males before being used for further genetic crosses and analysis. Strains containing *tba-1(ju89) dlk-1(tm4024)* were generated by crossing males carrying gene(s) of interest into CZ12121 [*tba-1(ju89) dlk-1(tm4024); juIs1*] hermaphrodites. All strains used in this study are summarized in Table 1.1 and are frozen down in collection.

Genotyping

Genotyping was performed using primers in targeted region to amplify genomic DNA from whole worm lysis with standard PCR techniques and analyzing amplicon in one of three ways: 1) analyzing band size in gel, 2)

sequencing PCR product and aligning against reference sequence in NCBI nucleotide BLAST (https://blast.ncbi.nlm.nih.gov/Blast.cgi), or 3) restriction enzyme digest. Primers used and genotyping strategy applied are summarized in Table 1.2.

Whole genome sequencing and genetic mapping

DNA of the originally isolated suppressing strain, CZ12371 [*tba-1(ju89) dlk-1(tm4024); ju983; juIs1*], was sent for whole genome sequencing (Beijing Genomics Institute BGI Americas). Raw sequencing data were analyzed using a custom workflow online at Galaxy [optimized for analysis by S. Cherra (unpublished)], and a list of unique SNPs caused by the mutagenesis were generated. We selected SNPs that resulted in the loss or gain of a restriction enzyme recognition site for use in linkage mapping.

ju983 was found to link to chromosome III or IV. First, Dr. Yan Dong generated the strain NYL132 by outcrossing the original strain, CZ12371, to *juIs1* males, recovering the *tba-1(ju89) dlk-1(tm4024)* in the F2 generation, and then re-isolating suppression in the F3 generation. Second, I analyzed CZ12371 and NY132 for the presence of selected SNPs. The process of outcrossing removes extraneous mutations that do not contribute to suppression. Thus, if a chosen SNP in CZ12371 is linked to suppression, it will be present in the outcrossed strain NYL132; and if a SNP is not linked to suppression, it may be found in the wild-type or heterozygous condition in the outcrossed strain.

I performed a second round of outcrossing using NYL132 and *juIs1* males, generating the strain CZ25496, and further linkage analysis mapped suppression to chromosome III in the region between -4.03 cM and +11.20 cM. Linkage analysis is summarized in Table 1.3.

Microscopy and synaptic phenotype scoring

Presynaptic terminals of GABAergic motor neurons were visualized using the transgene *juIs1* [$P_{unc\text{-}25}$*-SNB-1::GFP*], which tags the synaptic vesicle protein, synaptobrevin, with GFP. Individual puncta represent individual presynaptic terminals.

Wild-type animals at young adult stage have puncta along the dorsal and ventral nerve cords. However, DD-remodeling defective mutants such as CZ12121 [*tba-1(ju89) dlk-1(tm4024); juIs1*] will retain synapses along the ventral nerve cord, fail to form new synapses along the dorsal nerve cord (except near the head and tail), and accumulate synaptic vesicles in commissures. Animals were scored on DD-remodeling capability by looking for puncta towards the middle of the dorsal nerve cord and observance of GFP accumulated in commissures.

L4 animals for relevant strains were kept at 20°C overnight, one day before imaging and observation. Day one adults were then immobilized in 0.6 mM Levamisole and mounted on 10% agarose pads such that the ventral side of the animals was against the pad. Counts for number of synapses were taken by

counting puncta along the entire dorsal nerve cord using a Zeiss Axioplan 2 microscope equipped with Chroma HQ filters. Representative images were taken in similarly prepared animals using a Zeiss LSM 710 confocal microscope.

For transgenic rescue using *tbb-2(+)*, percentage of animals that successfully underwent DD-remodeling were counted in transgenic lines by looking for puncta in the dorsal nerve cord towards the middle of the worm. Three transgenic lines were established in the *juIs1* background (CZ25571-25573) and the *tba-1(ju89) dlk-1(tm4024); tbb-2(ju1535); juIs1* background (CZ25574-25576). Data were pooled for the three lines in each background.

Movement assay

Animals were scored on ability of both forward and backwards motion. DD-remodeling defective mutants are nearly paralyzed and coil dorsally when tapped on the head as described in Kurup et al., 2010. Animals were categorized as “uncoordinated” if they had severe deficits in forward motion that resembled the near-paralysis of remodeling-defective mutants and if tapping on the head caused dorsal coiling. Animals were categorized as “suppressed” if forward motion was achieved and if tapping the head produced backwards motion.

Statistical analysis

Statistical analysis was performed in GraphPad Prism 5.0. Significance was determined with an un-paired t-test for two samples and one-way ANOVA with Tukey's post-hoc test for multiple comparisons.

Results

ju1535 was a mutation in *tbb-2*

The mutation *ju983* was isolated in a suppressor screen in *tba-1(ju89) dlk-1(tm4024)*. After finding linkage to chromosome III, *ju983* was found to contain closely linked SNPs in three genes; and each SNP was then assigned with an allele designation, *ju1516, ju1517,* and *ju1535*, in the genes *nipa-1, golg-4,* and *tbb-2,* respectively.

nipa-1 encodes an orthologue of Drosophila *spichthyin*, a magnesium transporter involved in synapse formation at the neuromuscular junction and regulation of microtubule dynamics (Wang, Shaw, Tsang, Reid, & Kane, 2007). *ju1516* contains two mutations in the protein coding sequence of *nipa-1* (Figure 1.3 A). Dr. Yan Dong established two lines, NYL248 and NYL249, in which the suppressed strain *tba-1(ju89) dlk-1(tm4024); ju983; juIs1* carried extrachromosomal *nipa-1(+)* cDNA to see if suppression could be rescued. I checked both lines for DD-remodeling and found that the transgene could not rescue suppression. The two lines had the same number of synapses along the

dorsal nerve cord as the suppressor, NYL132 [*tba-1(ju89) dlk-1(tm4024); ju983; juIs1*] (Figure 1.3 B).

GOLG-4 is a member of the Golgin family of proteins involved in golgi targeting. These proteins function through a C-terminal GRIP domain (Munro, 2017). *golg-4(ju1517)* results in a premature STOP codon just inside the GRIP domain (Figure 1.4) and is thus likely a loss of function allele. To see if loss of the GRIP domain causes suppression, I crossed *gk601212*, a known loss-of-function allele that also results in a premature STOP before the GRIP domain (Figure 1.4), into *tba-1(ju89) dlk-1(tm4024)* and generated the triple mutant CZ# [*tba-1(ju89) dlk-1(tm4024); golg-4(gk601212); juIs1*]. These animals are uncoordinated to the same extent as *tba-1(ju89) dlk-1(tm4024)* and the DD-remodeling defect is not suppressed. We continued our investigation in *tbb-2(ju1535)*.

ju1535 is a C to T mutation in exon 3 of the beta-tubulin gene *tbb-2*. This mutation changes the conserved proline to serine (P305S). The amino acid change affects TBB-2 at an internal face in the folded protein (Figure 1.3).

Expression of wild-type *tbb-2* can rescue suppression

To confirm suppression is due to the mutation in *tbb-2* and not a neighboring SNP, we performed transgenic rescue using an extrachromosomal array carrying *tbb-2(+)*. Because the gene is small, ~1.8 kb, the entire genomic sequence was used instead of cDNA. The construct was injected into both wild-

type and suppressed strains. Overexpression of wild-type *tbb-2* did not affect DD-remodeling in WT animals and the lines with the suppressing mutation in the background, CZ25574-25576 [*tba-1(ju89) dlk-1(tm4024); tbb-2(ju1535); juIs1; Ex-TBB-2(+)*], were successfully rescued as animals carrying the transgene regained the DD-remodeling defect (Figure 1.4).

ju1535 suppresses *tba-1(ju89)* synaptic defects and DD-remodeling defects in *tba-1(ju89) dlk-1(tm4024)*

During the outcross of NYL132 to generate CZ25496, I isolated >200 recombinants that included those that also separated *tba-1(ju89)* from *dlk-1(tm4024)* at chromosome I. The resulting strain, CZ25355 [*tba-1(ju89); tbb-2(ju1535); juIs1*], did not show movement defects seen in *tba-1(ju89)* single animals and were nearly wild-type in appearance. After checking the synapses under the fluorescent compound microscope, I found that the *tba-1(ju89); tbb-2(ju1535)* double-mutants also had an increased number of synapses compared to *ju89* mutants (Figure 1.5). This finding indicates that *tbb-2(ju1535)* suppressed synapse defects of *tba-1(ju89).*

I then crossed *tbb-2(ju1535)* back into the *tba-1(ju89) dlk-1(tm4024)* background and found that it does suppress DD-remodeling defects. Triple mutants of *tba-1(ju89) dlk-1(tm4024); tbb-2(ju1535)* have restored forward movement and a significant increase in the number of synapses along the dorsal nerve cord in young adult animals (Figure 1.6 A,F).

ju1535 does not behave as a null allele of *tbb-2*

To determine whether *tbb-2(ju1535)* behaved as a loss-of-function mutation, I compared it to a null allele of *tbb-2*, *gk129. gk129* is a deletion that removes the start codon from the gene (Figure 1.3).

First, we compared the synapse pattern of the two *tbb*-2 alleles. *ju1535* showed a reduction in the number of synapses along the dorsal nerve cord whereas *gk129* was indistinguishable from wild-type. We then crossed *tbb-2(gk129)* into the *tba-1(ju89) dlk-1(tm4024)* background to see if the null allele of *tbb-2* would also suppress the DD-remodeling defect. However, the *tbb-2(gk129)*; *tba-1(ju89) dlk-1(tm4024)* triple-mutants did not suppress DD-remodeling (Figure 1.6) and these animals were just as uncoordinated and slow-growing as *tba-1(ju89) dlk-1(tm4024)*.

Interaction between *dlk-1* and *tbb-2*

We next investigated whether the *ju1535* could synergize with *dlk-1(tm4024)* and cause enhanced synaptic defects similar to those seen in *tba-1(ju89) dlk-1(tm4024)*. We crossed both *ju1535* and *gk129* into the *dlk-1(tm4024)* background and observed any synaptic phenotypes. *dlk-1(tm4024); tbb-2(ju1535)* animals showed no enhanced synaptic defects nor any behavioral phenotypes. These animals are phenotypically identical to *ju1535* animals. However, we saw that *dlk-1(tm4024); tbb-2(gk129)* animals were uncoordinated,

although not to the extent of the near-paralysis in *tba-1(ju89) dlk-1(tm4024)* animals. The *dlk-1(tm4024); tbb-2(gk129)* animals also appear to show a reduced number of synapses in the dorsal nerve cord.

TBB-2(JU1535) may hinder TBA-1(JU89) from being incorporated into microtubules

Double-mutants of *tba-1* and *tbb-2* null alleles are not viable, suggesting that TBB-2 is the preferred binding partner for TBA-1 (Baran et al., 2010). We hypothesize that *tbb-2(ju1535)* suppresses *tba-1(ju89)* by binding the mutant alpha-tubulin and preventing it from being incorporated into the microtubule. In this way, fewer microtubules are affected by the mutant alpha-tubulin and animals are therefore suppressed. To investigate this question, I generated the strain CZ26048 [*tba-1(ok1135); tbb-2(ju1535); Prgef-mKate2-TBA-1(ju89)*] and compared it to CZ22972 [*tba-1(ok1135); Prgef-mKate2-TBA-1(ju89)*] to see if there was a change in localization or expression. Preliminary observations do not reveal any striking differences between the strains, but careful quantification has not been made.

Discussion

ju1535 is a gain-of-function mutation in beta-tubulin

Our data show that *ju1535* behaves very differently from the null allele of *tbb-2*. Where the null does not have any synaptic phenotypes, *ju1535* causes a reduction in the number of synapses along the dorsal nerve cord. Furthermore, the null does not suppress the DD-remodeling defects in *tba-1(ju89) dlk-1(tm4024)* while *ju1535* does. Taken together, our data shows that *ju1535* is a gain-of-function mutation because it does not behave as wild-type *tbb-2* nor a null allele of *tbb-2*.

An interaction between *tbb-2* and *dlk-1*

Because *ju1535* causes a reduction in the number of synapses similar to the reduction seen in *ju89* mutants, we thought that it could perhaps synergize with *dlk-1(tm4024),* too. However, the double did not show any remodeling phenotype and the animals appeared as *ju1535* alone. The *tbb-2* null allele was crossed into the *dlk-1(tm4024)* background as well. These animals became uncoordinated and have fewer synapses along the dorsal nerve cord by observation. However, the extent of defects seen in *dlk-1(tm4024); tbb-2(gk129)* have not been quantified.

Tables

Table 1.1: Strain list

Strain number	Genotype	Source/notes
CZ333	*P_{unc-25}-SNB-1::GFP (juIs1) IV*	
CZ1018	*tba-1(ju89) I; P_{unc-25}-SNB-1::GFP (juIs1) IV*	
CZ12121	*tba-1(ju89) dlk-1(tm4024) I; P_{unc-25}-SNB-1::GFP (juIs1) IV*	
CZ12371	*tba-1(ju89) dlk-1(tm4024) I; ju983 III; P_{unc-25}-SNB-1::GFP (juIs1) IV*	*ju983* encompasses *nipa-1(ju1516) golg-4 (ju1517) tbb-2(ju1535)*
CZ22972	*tba-1(ok1135) I; P_{flp-13}-SNB-1::GFP (juIs137) III ; Prgef-mKate-TBA-1(JU89) (juEx7003)*	
CZ25353	*golg-4(gk601212) III*	
CZ25354	*tba-1(ju89) I; nipa-1(ju1516) golg-4(ju1517) III; P_{unc-25}-SNB-1::GFP (juIs1) IV*	
CZ25355	*tba-1(ju89) I; tbb-2(ju1535) III; P_{unc-25}-SNB-1::GFP (juIs1) IV*	
CZ25356	*tba-1(ju89) dlk-1(tm4024) I; golg-4(gk601212) III; P_{unc-25}-SNB-1::GFP (juIs1) IV*	
CZ25357	*tba-1(ju89) dlk-1(tm4024) I; nipa-1(ju1516) golg-4(ju1517); P_{unc-25}-SNB-1::GFP (juIs1) IV*	
CZ25358	*nipa-1(ju1516) golg-4(ju1517) III; P_{unc-25}-SNB-1::GFP (juIs1) IV*	
CZ25359	*tba-1(ju89) dlk-1(tm4024) I; tbb-2(ju1535) III; P_{unc-25}-SNB-1::GFP (juIs1) IV*	
CZ25360	*tbb-2(ju1535) III; P_{unc-25}-SNB-1::GFP (juIs1) IV*	
CZ25496	*tba-1(ju89) dlk-1(tm4024) I; ju983 III; P_{unc-25}-SNB-1::GFP (juIs1) IV*	
CZ25564	*tbb-2(gk129) III; P_{unc-25}-SNB-1::GFP (juIs1) IV*	
CZ25565	*tba-1(ju89) dlk-1(tm4024) I; tbb-2(gk129) III; P_{unc-25}-SNB-1::GFP (juIs1) IV*	

(Table 1.1 continued)

CZ25571	*P_{unc-25}-SNB-1::GFP (juIs1) IV; PCR8::TBB-2(genomic) (juEx7692)*	
CZ25572	*P_{unc-25}-SNB-1::GFP (juIs1) IV; PCR8::TBB-2(genomic) (juEx7693)*	
CZ25573	*P_{unc-25}-SNB-1::GFP (juIs1) IV; PCR8::TBB-2(genomic) (juEx7694)*	
CZ25574	*tba-1(ju89) dlk-1(tm4024) I; tbb-2(ju1535) III; P_{unc-25}-SNB-1::GFP (juIs1) IV; PCR8::TBB-2(genomic) (juEx7695)*	
CZ25575	*tba-1(ju89) dlk-1(tm4024) I; tbb-2(ju1535) III; P_{unc-25}-SNB-1::GFP (juIs1) IV; PCR8::TBB-2(genomic) (juEx7696)*	
CZ25576	*tba-1(ju89) dlk-1(tm4024) I; tbb-2(ju1535) III; P_{unc-25}-SNB-1::GFP (juIs1) IV; PCR8::TBB-2(genomic) (juEx7697)*	
CZ25616	*dlk-1(tm4024) I; tbb-2(gk129) III; P_{unc-25}-SNB-1::GFP (juIs1) IV*	
CZ25617	*dlk-1(tm4024) I; mec-7-GFP (muIs32) II; tbb-2(gk129) III*	
CZ25618	*dlk-1(tm4024) I; tbb-2(ju1535) III; P_{unc-25}-SNB-1::GFP (juIs1) IV*	
CZ25619	*dlk-1(tm4024) I; mec-7-GFP (muIs32) II; tbb-2(ju1535) III*	
CZ	*tba-1(ju89) dlk-1(tm4024) I; mec-7-GFP (muIs32) II; nipa-1(ju1516) III*	
CZ	*tba-1(ok1135) I; tbb-2(ju1535) III; Prgef-mKate-TBA-1(JU89)*	
NYL132	*tba-1(ju89) dlk-1(tm4024) I; ju983 III; P_{unc-25}-SNB-1::GFP (juIs1) IV*	outcrossed from CZ12371
NYL248	*Ex-nipa-1(+); tba-1(ju89) dlk-1(tm4024) I; ju983 III; P_{unc-25}-SNB-1::GFP (juIs1) IV*	
NYL249	*Ex-nipa-1(+); tba-1(ju89) dlk-1(tm4024) I; ju983 III; P_{unc-25}-SNB-1::GFP (juIs1) IV*	
NYL271	*mec-7-GFP (muIs32) II; nipa-1(ju1516) III; pmk-3(ok169) IV*	

Table 1.2: Genotyping primers

Gene(allele)	mutation	restriction enzyme site loss or gain	analysis	detection	Primer name	Sequence (5'→3')
tba-1(ju89)	C→T point mutation	none	sequencing	WT: C	YJ9560	CGACAACGAGGCTATCTATG
				ju89: T	YJ9661	TCGTATACAACACAAGCGATG
tba-1(ok1135)	900 bp deletion	none	gel	WT: 555 bps	YJ11190	GGGCACTTGAAGTTGATGGT
				ok1135: ~1443 bps	YJ11191	CCTTTCCTCGCACCAGAATA
					YJ12028	GCTTGGACTACAAGTTCGATC
dlk-1(tm4024)	460 bp deletion	none	gel	WT: 527 bps	YJ11008	GTGAGTTTTAAATATTTTTTTTTGATTGAAAATTC
				tm4024: 843 bps	YJ11009	GGTGTTGGAACAAAGTGAGTTG
					YJ11010	AGGCTAGTTTCAGGTTTGGTC
nipa-1(ju1516)	G→A point mutation	NsiI site loss	enzyme digest	WT: 822 + 289 bps	YJ12126	CGCGGAGCCACATAGACAACG
				ju1516: 1111 bps	YJ12127	CGAATTCAGCCGGTGTGGAGC
golg-4(gk601212)	C→T point mutation	Hpy8I site gain	enzyme digest	WT: 668 bps	YJ12074	GCGAAGAAGGAGCTTGAAGC
				gk601212: 550 + 118 bps	YJ12076	CAGCGTCGCTGATTGGTAG
golg-4(ju1517)	A→T point mutation	HindIII site loss	enzyme digest	WT: 312 + 134 bps	YJ12091	GAGTCATCGAGTTTTGGCAG
				ju1517: 446 bps	YJ12092	CCGGATCAGCAATTCCGTG
tbb-2(gk129)	766 bp deletion	none	gel	WT: 1143 bps	OKK276	GCTGCATGTCTGCTCCTACA
				gk129: 403 bps	OKK277	TCGGTGTTCTCAACAAGCTG
tbb-2(ju1535)	G→A point mutation	none	sequencing	WT: G	YJ12085	GCCTTGCGGCGGAACATAG
				ju1535: A	YJ12086	ACAGCTCAATGCCGATCTCCG

Table 1.3: Summary of linkage analysis for *ju1535*

Chr.	genetic position (cM)	nt	Δ nt	restriction site loss/gain	gene	WT	CZ 12371	NYL 132
II	+1.82	C	T	Cac81 loss	*R53.2*	329 + 163 bps	492 bps	329 + 163 bps
III	-6.96	G	A	NsiI loss	*nipa-1*	822 + 289 bps	1111 bps	1111 bps
	+11.20	G	A	seq	*Y66D12A.1*	G	A	G
IV	~+5.00	G	A	BstYI loss	*ZK822.4*	512 + 243 bps	756 bps	756 bps
V	~+2.50	G	A	NspI loss	*AC3.5*	748 + 197 bps	945 bps	748 + 197 bps
X	-1.82	C	T	TspGWI loss	*lam-2*	143 + 519 bps	662 bps	143 + 519 bps

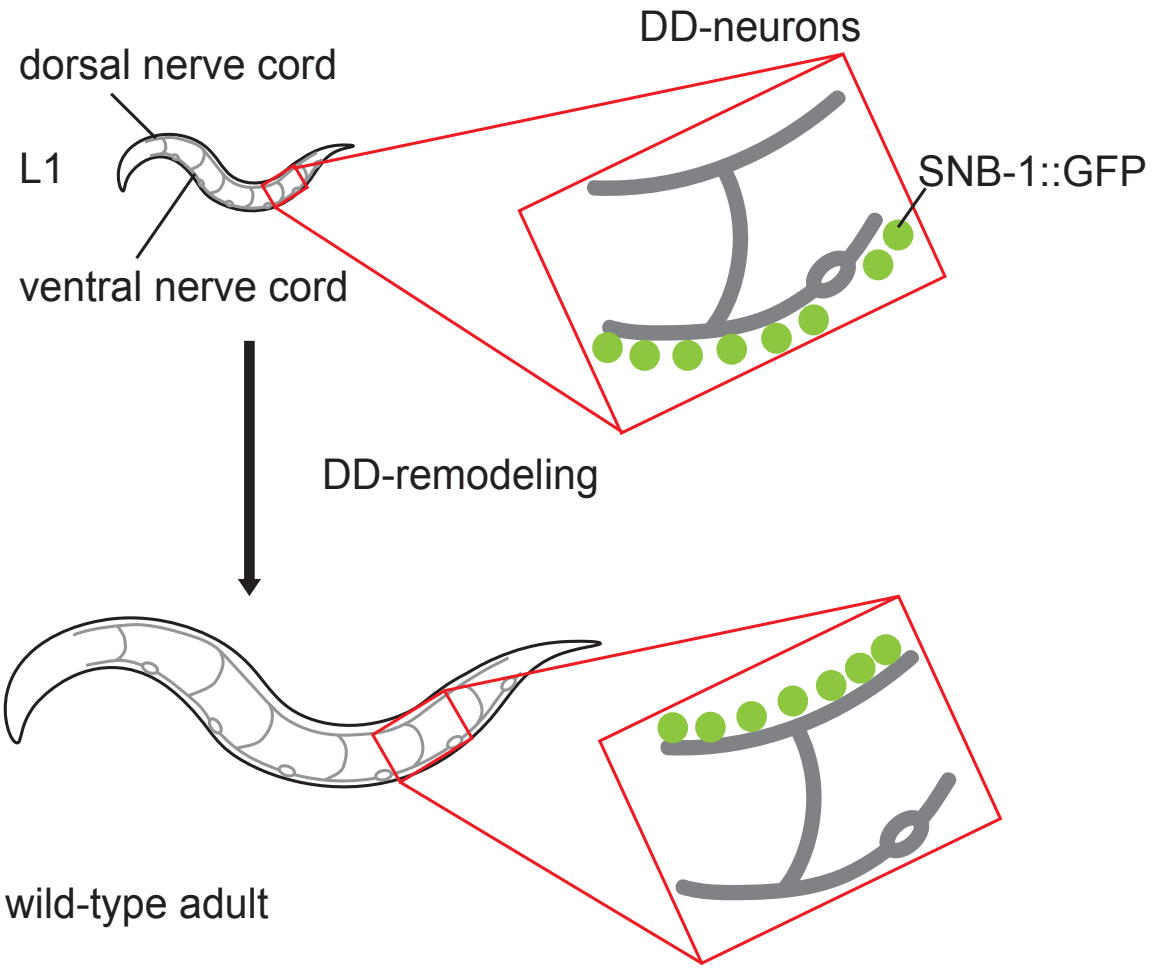

Figure 1.1: C. elegans undergo circuit rewiring at an early larval stage I DD-remodeling occurs in L1 stage in *C. elegans*. Highlighted in the red box are DD neurons. Synapses in pre-synaptic neuron are represented by green circles.

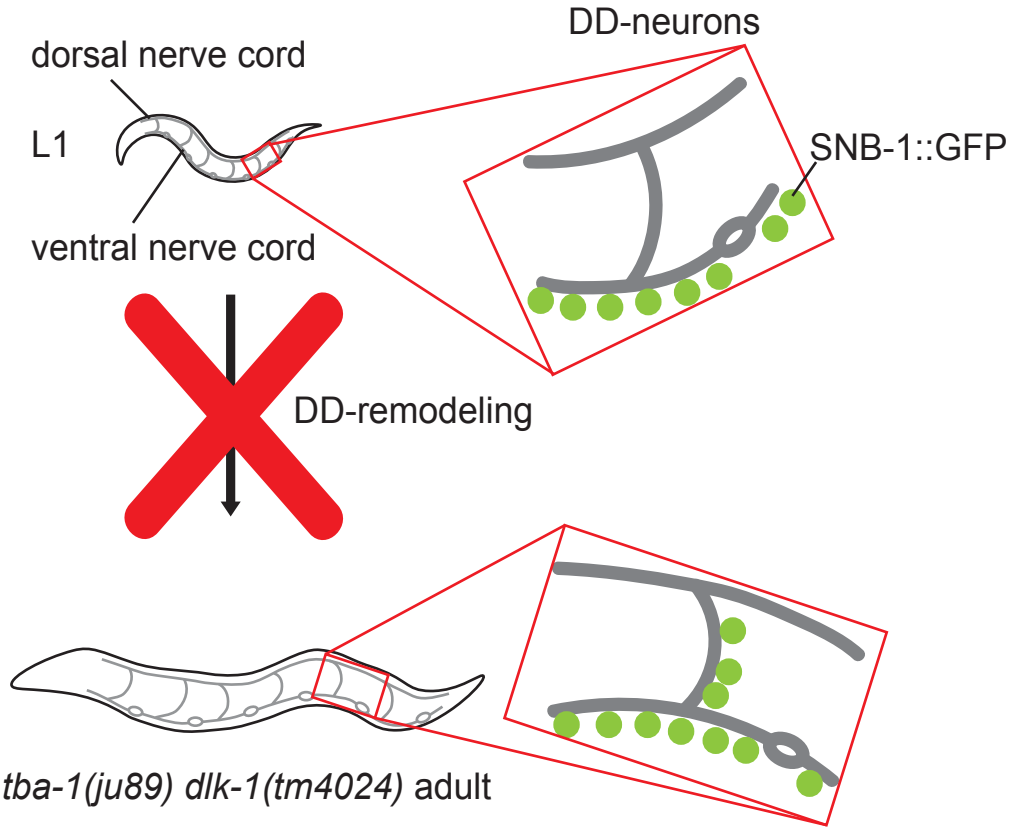

Figure 1.2: DD-remodeling is blocked in tba-1(ju89) dlk-1(tm4024) double mutants | DD-remodeling fails in *tba-1(ju89) dlk-1(tm4024)* animals. Synaptic vesicles get stuck in commissures and fail to establish real synapses along the dorsal nerve cord.

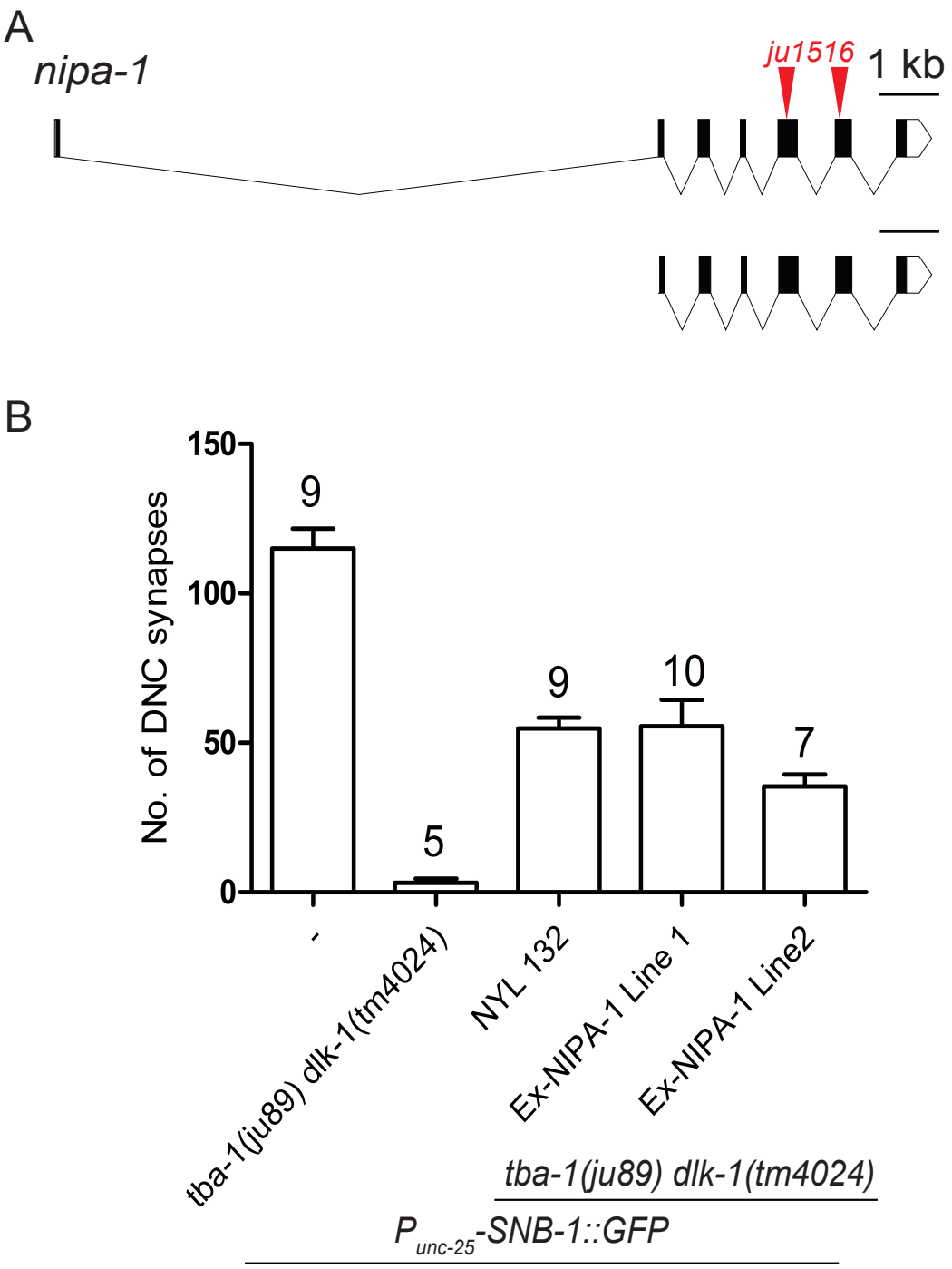

Figure 1.3: nipa-1(ju1516) is not causative for suppression | **A** *nipa-1* gene structure with *ju1516* mutations annotated in red. **B** Quantification of synapses in suppressed and rescued lines. Error bars represent SEM. Number of animals scored (n) plotted above corresponding bar.

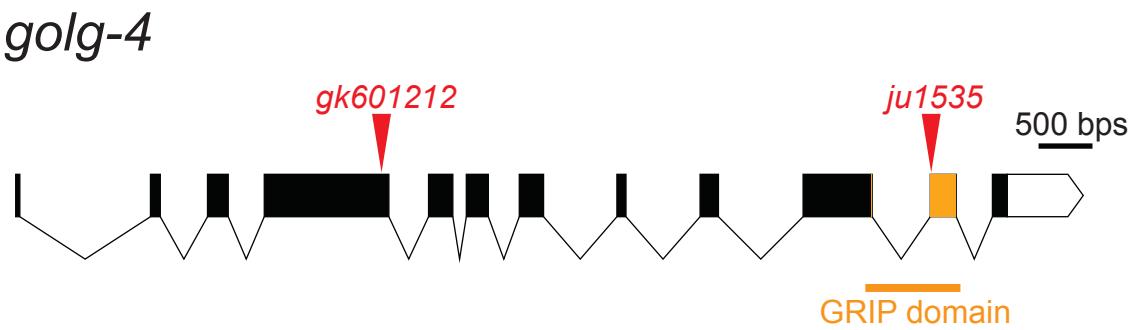

Figure 1.4: golg-4(ju1517) is not causative for suppression **|** *golg-4* gene structure. Functional GRIP domain highlighted in orange. *gk601212* and *ju1535* loss-of-function mutations annotated in red.

A

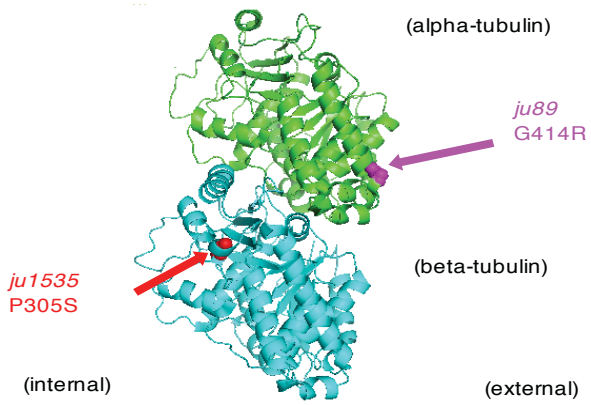

B

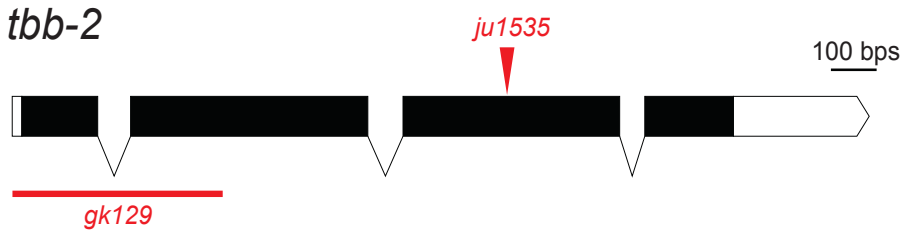

C

```
C.e. TBB-2    AACDPRHGRYLTVAAMFRGRMSMREVDEQMLNVQNKNSSYFVEWIPNNVKTAVCDIPPRG 360
H.s. TBB4B    AACDPRHGRYLTVAAVFRGRMSMKEVDEQMLNVQNKNSSYFVEWIPNNVKTAVCDIPPRG 360
M.m. Tubb4b   AACDPRHGRYLTVAAVFRGRMSMKEVDEQMLNVQNKNSSYFVEWIPNNVKTAVCDIPPRG 360
```

Figure *1.5: ju1535 is a point mutation in tbb-2* **I A** Crystal structure of the alpha- (green) and beta-tubulin (blue) heterodimer. *ju89* noted in purple and *ju1535* noted in red. **B** *tbb-2* gene structure. *gk129* deletion removes the start codon from the coding sequence. *ju1535* is a point mutation C → T in exon 3. **C** Protein sequencing alignment for *C. elegans,* human, and mouse TBB-2. Mutated proline305 highlighted in red.

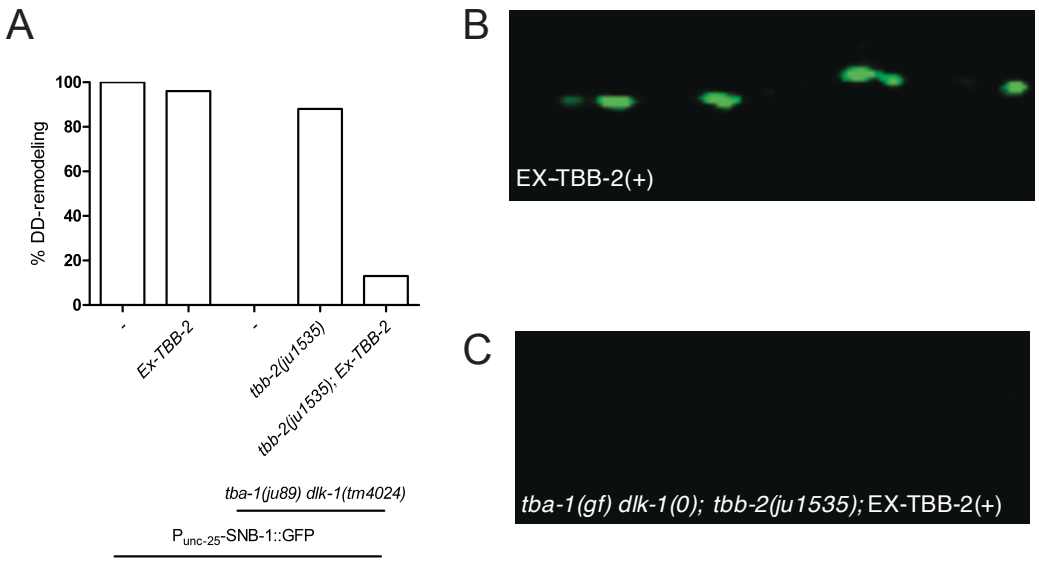

Figure 1.6: ju1535 is rescued by tbb-2(+) I **A** Percentage of animals that successfully underwent DD-remodeling. 90 total animals scored for transgenic lines, 30 animals per established line. **B, C** Representative images of animals carrying transgene in the wild-type (B) and suppressed [*tba-1(ju89) dlk-1(tm4024); tbb-2(ju1535)*] backgrounds (C).

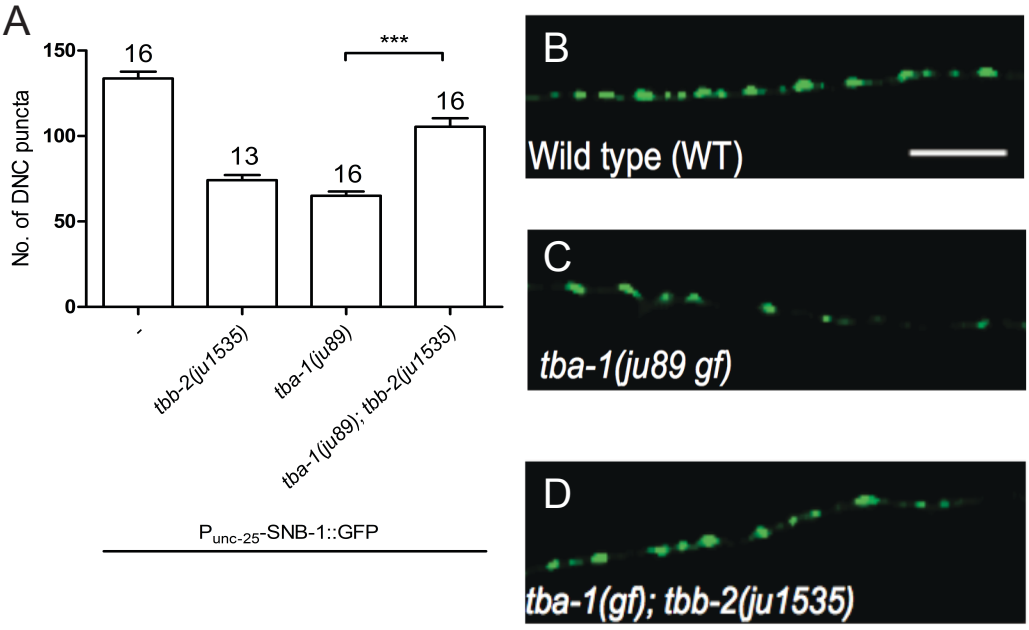

Figure 1.7: ju1535 suppresses tba-1(ju89) **I A** Number of dorsal nerve cord synapses. Number of animals scored (n) plotted above corresponding bar. Error bars represent SEM. **B-D** Representative images of dorsal nerve cord synapses visualized using P_{unc-25}-SNB-1::GFP. Scale bar (B, white bar) represents 10 µm.

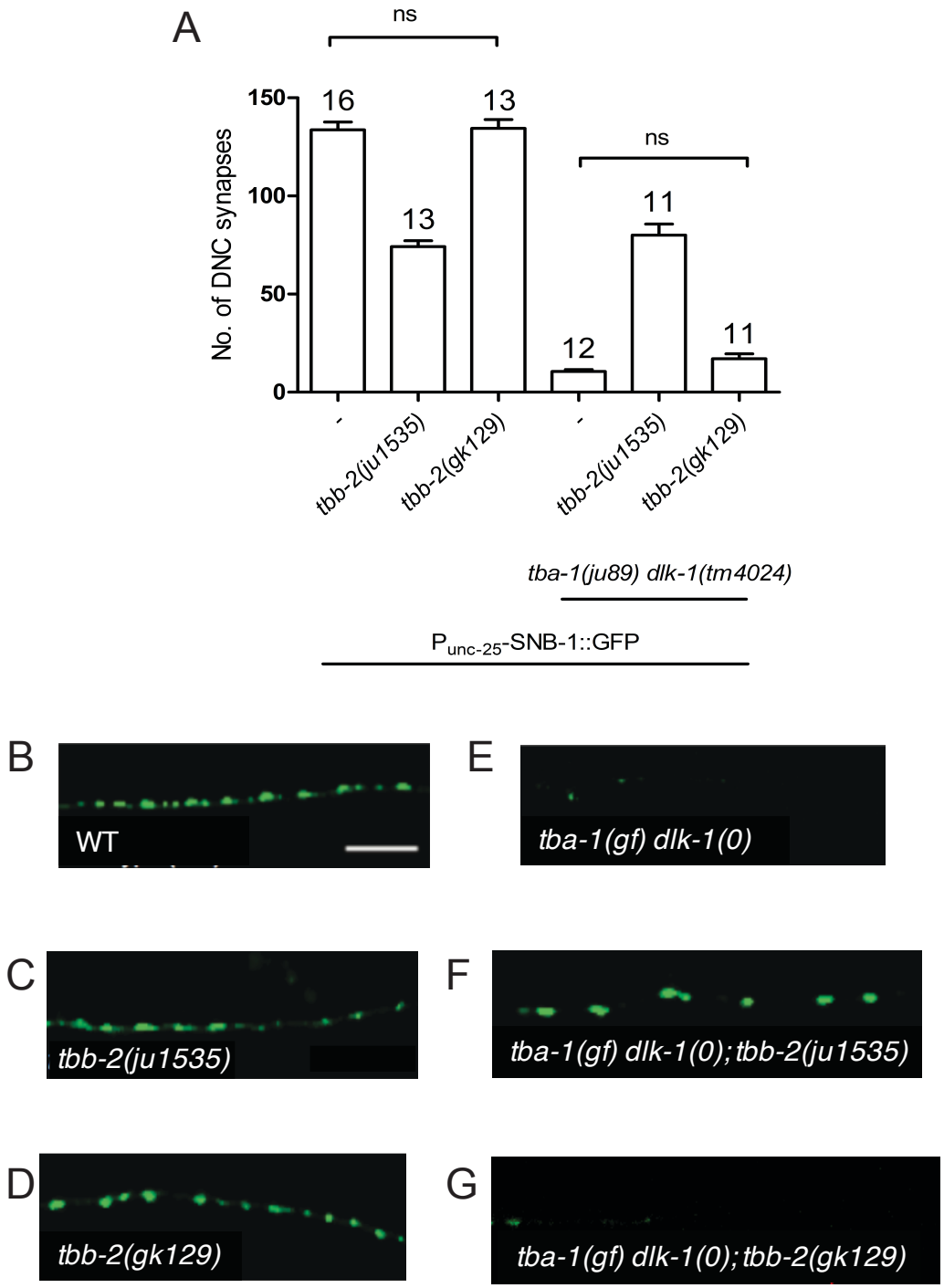

Figure 1.8 ju1535 does not behave as a tbb-2 null allele **I A** Comparison of the number of dorsal nerve cord synapses. Number of animals scored (n) plotted above corresponding bars. Error bars represent SEM. **B-G** Representative images of dorsal nerve cord synapses visualized using P_{unc-25}-SNB-1::GFP. Scale bar (B, white bar) represents 10 µm.

CHAPTER 2: Genetic suppressor screen of a synapse-defective alpha-tubulin mutant

Background

The gain-of-function mutation *ju89* occurs at the C-terminus of TBA-1, the domain of the protein involved in binding microtubule-associated proteins (Figure 0.1). Thus, the mutation causes the synaptic defects and uncoordinated motion at the sub-cellular level by disrupting microtubule-associated proteins ability to bind and regulate microtubules.

To further identify microtubule-associated proteins that are needed for proper synapse formation, we performed a screen in *tba-1(ju89)* and picked suppressors that ameliorated the locomotor defects. However, we found that suppressors can be picked based on behavior while leaving synaptic defects in DD neurons unaltered.

Materials and methods

Strain maintenance and genetic screen

All strains were maintained on NGM plates as described in Brenner, 1974. Plates were kept on the benchtop at 22°C. All strains used in this study are summarized in Table 2.1

Two genetic screens were performed; one in CZ2411 [*tba-1(ju89); juIs137*], and a second in CZ23343 [*tba-1(ju89); juIs137; juSi292*]. Screen design and details are illustrated in Figure 2.1 and 2.2. In brief, early L4s from the starting strain were treated with 47mM EMS for 4 hours. Twenty healthy late-L4s/young-adults were singled out onto separate plates from the treated animals as P0s and allowed to lay eggs. P0s were moved to fresh plates every 6-8 hours, after laying 10-20 eggs, totaling ~2,700 mutagenized haploid genomes in the *tba-1(ju89)* background and ~4,000 mutagenized haploid genomes in the *tba-1(ju89); juSi292* background. Suppressors were isolated from F2 generation by selecting for improved forward movement. Original isolates and additional strains generated therefrom by outcross to CZ2060 [$P_{flp\text{-}13}$*-SNB-1::GFP(juIs137)*] males are summarized in Table 2.2. All strains are frozen down in collection.

Genotyping, whole-genome sequencing, and genetic mapping

Genotyping was performed using primers in targeted region to amplify genomic DNA from whole-worm lysis with standard PCR techniques and analyzing amplicon in one of three ways: 1) analyzing band size in gel, 2) sequencing PCR product and aligning against reference sequence in NCBI nucleotide BLAST (https://blast.ncbi.nlm.nih.gov/Blast.cgi), or 3) restriction enzyme digest. Primers used and genotyping strategy applied are summarized in Table 2.3.

For whole-genome sequencing, genomic DNA was prepared from five 10-centimeter plates (1 mL of animals) for both CZ24004 and CZ24312 using Gentra Puregene Kit. Purified DNA was analyzed for each strain at Beijing Genomics Institute (BGI Americas). The obtained sequence data were aligned and compared to an in-lab Bristol N2 reference sequence, generating a list of unique single nucleotide polymorphisms (SNPs) using a Galaxy workflow [optimized for analysis by S. Cherra (unpublished)]. These SNPs were common between CZ24004 and CZ24312, but differed from the N2 reference.

To further map the causative mutation, we then outcrossed CZ24312 to CZ2060 [$P_{flp\text{-}13}$-*SNB-1::GFP(juIs137)*] males, obtaining the suppressor strain CZ25458. We performed linkage analysis using the identified SNPs, detected by a loss or gains of restriction enzyme site or by sequencing. A summary of linkage analysis is found in Table 2.4. However, analysis failed to link suppression to a specific SNP.

Microscopy and neuronal phenotype scoring

Presynaptic terminals of DD-neurons were visualized using the transgene *juIs137* [$P_{flp\text{-}13}$-*SNB-1::GFP*], which tags the synaptic vesicle protein, synaptobrevin, with GFP. Individual, round localizations of GFP, i.e. puncta, represent individual presynaptic terminals. Synaptic phenotypes were scored by comparing the shape and number of puncta along the dorsal nerve cord in

relevant strains against the wild-type CZ2060 [$P_{flp\text{-}13}$-*SNB-1::GFP(juIs137)*] and synapse-defective strain CZ2411 [*tba-1(ju89); juIs137*].

L4 animals for relevant strains were kept at 20°C overnight, one day before imaging and observation. Day one adults were then immobilized in 0.6 mM Levamisole and mounted on 10% agarose pads such that the ventral side of the animals was against the pad. Counts for number of synapses were taken by counting puncta along the entire dorsal nerve cord using a Zeiss Axioplan 2 microscope equipped with Chroma HQ filters. Representative images were taken in similarly prepared animals using a Zeiss LSM 710 confocal microscope.

Axon outgrowth was visualized using the transgene *juIs76* ($P_{unc\text{-}25}$-*GFP*) which expresses free GFP under a GABAergic neuron specific promoter. Synapses were simultaneously visualized in these animals with mCherry-tagged-RAB-3 using the transgene *juIs231* ($P_{unc\text{-}25}$-*RAB-3::mCherry*). Observations were made on Zeiss Axioplan 2 microscope equipped with Chroma HQ filters.

Movement assay

Animals were gently tapped on the head using a worm pick to assess ability of locomotion. Animals were then observed for voluntary forward motion. In the suppressors screen, animals were categorized as “uncoordinated” if forward motion closely resembled *tba-1(ju89)* mutants in which movement lacks the characteristic sinusoidal wave pattern and is slower and labored. Animals were categorized as “suppressed” if forward motion more closely resembled the

uniform waves observed in wild-type animals and was faster than *tba-1(ju89)* animals.

Statistical analysis

Statistical analysis was performed in GraphPad Prism 5.0. Significance was determined with an un-paired t-test for two samples and one-way ANOVA with Tukey's post-hoc test for multiple comparisons.

Results

Screen in *tba-1(ju89)* identified five suppressors

Using EMS mutagenesis, we performed a forward genetic screen in CZ2060 animals [*tba-1(ju89); juIs137*]. Based on improved forward movements, we isolated five suppressors (Table 2.2). Although all five suppressors improved forward movement, none significantly improved synapse morphology.

We attempted to outcross four of the five suppressors. We were unable to re-isolate suppression in *ju1381* and the other three did not show any improvement in suppression following the outcross.

We then sequenced each of the suppressors for additional mutations within *tba-1*. *ju1384* contained an additional mutation in *tba-1* resulting in a leucine to phenylalanine amino acid change.

Because suppression was weak in all five suppressors, and none greatly restored normal synapse morphology to *tba-1(ju89)* mutants, we continued our investigation by screening for suppressors in a different genetic background.

juSi292 is a two-copy insertion of genomic *tba-1(ju89)* at chromosome IV

Dr. Naina Kurup designed a construct that carried *tba-1(ju89)* genomic sequence and inserted it within chromosome IV (Figure 2.3). We hoped that, firstly, by increasing the number of copies of *tba-1(ju89)*, we would also see an increase in behavioral and synaptic defects, making the screen for suppressors easier. Secondly, the extra copies would reduce the chances of picking an intragenic suppressor because the chance of obtaining additional mutations in each copy is highly unlikely and therefore, animals would still be uncoordinated even if one copy of *tba-1(ju89)* was mutagenized.

As expected, animals with the extra copies show an increase in behavior defects. There was also a reduction in the number of synapse number (Figure 2.4 A-D). However, the double-copy insertion in the wild-type background did not appear to contribute any synaptic nor behavioral defects. In fact, these animals appear indistinguishable from wild-type (Figure 2.4 E)

To see if the reduction was due to a failure of the axons to grow fully along the nerve cord, we used $P_{unc\text{-}25}$*-GFP (juIs76)* to visualize axons. These animals showed an increase in the number of commissure defects per animal than observed in *tba-1(ju89)* single mutants (Figure 2.5).

A suppressor screen in *tba-1(ju89); juSi292*

The screen was carried out using CZ23343 [*tba-1(ju89); juSi292; juIs137*] as the starting strain. Although the extra copies did cause more severe motor defects, we only isolated two suppressors (Table 2.2).

Both suppressors improved forward movement in *tba-1(ju89); juSi292* background and also improved synaptic phenotypes. However, after outcross to remove the extra copies, only *ju1388* suppressed the *tba-1(ju89)* synapse defects (Figure 2.6). *ju1377*, although a strong behavioural suppressor, did not improve synapse morphology nor increase synapse number in the *tba-1(ju89)* single mutant background.

Discussion

Expression of *juSi292*

Because the extra copies of *ju89* in the wild-type background do not cause any phenotype similar to *ju89* at the endogenous locus, it would appear that the extra copies are not expressed and therefore not contributing. However, in a *tba-1* null background using the deletion allele *ok1135*, animals are mildly uncoordinated suggesting that there is expression of *juSi292*, albeit low. A quantification on the synaptic phenotype of this genetic combination has not been made. A possible explanation is that the insertion is in chromosome IV at a

region that does not contain many genes, and thus that area is condensed and less expressed overall. Another possible explanation is that the insertion is missing some regulatory element necessary for normal *tba-1* expression levels. The construct uses the full promoter sequence of *tba-1* but may be missing upstream or downstream regions that contribute to its normal expression profile at the endogenous locus. To see if adding extra copies of *tba-1(ju89)* increases expression, the level of transcription should be checked by q-RT PCR. This will tell whether the level of transcripts is increased in the insertion. However, this will not tell whether translation or degradation plays a role.

Suppressing *tba-1(ju89);juSi292* defects but not *tba-1(ju89)*

ju1387 suppressed only the more severe defects in *tba-1(ju89) juSi292*. Following outcross to remove the extra copies of *tba-1(ju89),* animals showed no suppression of the synaptic defects of *tba-1(ju89)* on its own. It is possible that suppression from *ju1387* is due to a mutation in a gene that is involved in regulating expression of the region of chromosome IV holding the insertion.

Separation between the uncoordinated phenotype and synaptic defects

Many of the suppressors isolated from these two screens were behavioral suppressors but, after visualizing synapses in these mutants, we found that the synaptic defects were not suppressed. Because we were only visualizing synapses in DD-neurons, we do not know how other neurons were affected by

the suppressing mutations. A possibility could be that the mutations affect different pathways that are compensating for the defects in DD neurons.

ju1388 may be linked to chromosome I or X

ju1388 was sent for whole genome sequencing and SNPs were picked at spaced locations along each chromosome. Early linkage analysis seemed to suggest that the causative mutation was located on chromosome V, as that entire mutagenized chromosome was maintained through the first round of outcross (Table 2.6). However, a second round of outcross showed that some suppressed progeny completely replaced chromosome V with a wild-type copy. Regions of chromosome I and chromosome X were also maintained through the outcross, however, and may contain the causative mutation for suppression.

Tables

Table 2.1: Strain list

Strain number	Genotype	Notes
CZ2060	*P_{flp-13}-SNB-1::GFP (juIs137) III*	
CZ2411	*tba-1(ju89) I; P_{flp-13}-SNB-1::GFP (juIs137) III*	
CZ23826	*ju1381; tba-1(ju89) I; P_{flp-13}-SNB-1::GFP (juIs137) III*	
CZ23829	*ju1382; tba-1(ju89); P_{flp-13}-SNB-1::GFP (juIs137) III*	
CZ23830	*tba-1(ju1383, ju89) I; P_{flp-13}-SNB-1::GFP (juIs137) III*	
CZ23831	*ju1384; tba-1(ju89) I; P_{flp-13}-SNB-1::GFP (juIs137) III*	
CZ23832	*ju1385; tba-1(ju89) I; P_{flp-13}-SNB-1::GFP (juIs137) III*	
CZ24308	*ju1385; tba-1(ju89) I; P_{flp-13}-SNB-1::GFP (juIs137) III*	outcrossed CZ23832 to CZ2060 (*juIs137*) males
CZ24309	*ju1385; tba-1(ju89) I; P_{flp-13}-SNB-1::GFP (juIs137) III*	outcrossed CZ24308 to CZ2060 (*juIs137*) males
CZ24001	*tba-1(ju89) ; P_{flp-13}-SNB-1::GFP (juIs137) III; PCFJ201-TBA-1(ju89)fullgenomicsequence(juSi292) IV*	
CZ24003	*ju1387; tba-1(ju89) ; P_{flp-13}-SNB-1::GFP (juIs137) III; PCFJ201-TBA-1(ju89)fullgenomicsequence(juSi292) IV*	
CZ24004	*ju1388; tba-1(ju89) ; P_{flp-13}-SNB-1::GFP (juIs137) III; PCFJ201-TBA-1(ju89)fullgenomicsequence(juSi292) IV*	
CZ24311	*ju1387; tba-1(ju89) ; P_{flp-13}-SNB-1::GFP (juIs137) III*	
CZ24312	*ju1388; tba-1(ju89) ; P_{flp-13}-SNB-1::GFP (juIs137) III*	
CZ24313	*dlk-1(tm4024); P_{flp-13}-SNB-1::GFP (juIs137) III; PCFJ201-TBA-1(ju89)fullgenomicsequence(juSi292) IV*	

(Table 2.1 continued)

CZ24582	*tba-1(ju1383, ju89) I; P_{flp-13}-SNB-1::GFP (juIs137) III*	outcrossed CZ23830 to CZ2060 (*juIs137)* males
CZ24583	*tba-1(ok1135) ; P_{flp-13}-SNB-1::GFP (juIs137) III; PCFJ201-TBA-1(ju89)fullgenomicsequence(juSi292) IV*	
CZ24584	*tba-1(ok1135) dlk-1(tm4024) I; P_{flp-13}-SNB-1::GFP (juIs137) III*	
CZ24587	*P_{unc-25}-RAB-3::mcherry (juIs231); tba-1(ju89) dlk-1(tm4024) I; P_{unc-25}-GFP (juIs76) II*	
CZ24588	*P_{unc-25}-RAB-3::mcherry (juIs231); tba-1(ju89) I; P_{unc-25}-GFP (juIs76) II; PCFJ201-TBA-1(ju89)fullgenomicsequence(juSi292) IV*	

Table 2.2: Mutations isolated from suppressor screens

starting strain	mutations isolated	assigned strain number	notes
CZ2411 (*tba-1(ju89); juIs137*)	*ju1381*	CZ23828	attempted to outcross – unable to re-isolate suppression
	ju1382	CZ23829	un-outcrossed
	ju1383	CZ23830	outcrossed to *juIs137* males
	ju1384	CZ23831	outcrossed to *juIs137* males intragenic suppressor
	ju1385	CZ23832	outcrossed to *juIs137*
CZ23343 (*tba-1(ju89);juIs137;juSi292*)	*ju1387*	CZ24003	outcrossed to *juIs137* and removed insertion at chromosome IV
	ju1388	CZ24004	outcrossed to *juIs137* and removed insertion at chromosome IV

Table 2.3: Genotyping primers

Gene(allele)	mutation	analysis	detection	Primer name	Sequence (5'→3')
tba-1(ju89)	C→T point mutation	sequencing	WT: C	YJ9560	CGACAACGAGGCTATCTATG
			ju89: T	YJ9661	TCGTATACAACACAAGCGATG
tba-1(ok1135)	900 bp deletion	gel	WT: 555 bps	YJ11190	GGGCACTTGAAGTTGATGGT
			ok1135: ~1443 bps	YJ11191	CCTTTCCTCGCACCAGAATA
				YJ12028	GCTTGGACTACAAGTTCGATC
juSi292	14 kb insertion	gel	WT: 623 bps	YJ12026	CGACAACGAGGCTATCTATG
			juSi292: 1039 bps	YJ12027	CGGGAAGTTAAGCGTCATTG
				YJ12028	GCTTGGACTACAAGTTCGATC

Table 2.4: Summary of chromosomal linkage analysis for *ju1388*

Chr.	genetic position (cM)	nucleotide position	nt	Δ nt	restriction site loss/gain or sequence	gene	WT	CZ 24004 original isolate	CZ 25458 outcrossed
I	-0.28	5198492	G	A	seq	*pde-5*	G	A	G
	+13.24	12489793	G	A	seq	*pars-2*	G	A	A
II	-4.36	4463162	G	A	MfeI loss	*vps-18*	326 + 729 bps	1055 bps	326 + 729 bps
	--	11037934	C	T	NgoMIV loss	*F33A8.10*	335 + 172 bps	507 bps	335 + 172 bps
	--	12857833	C	T	BanII loss	*Y46G5A.29*	243 + 342 bps	585 bps	243 + 342 bps
III	-0.05	8810977	C	G	HaeII loss	*pat-2*	243 + 213 bps	456 bps	243 + 213 bps
	+16.32	12289300	C	T	HaeIII loss	*mrp-8*	297 + 144 bps	441 bps	297 + 144 bps
	+21.21	13303626	C	T	HhaI loss	*klp-19*	297 + 454 bps	751 bps	297 + 454 bps
IV	+3.14	6297260	C	T	seq	*srv-27*	C	T	C
	+12.39	14710711	T	A	seq	*lgc-7*	T	A	T
V	-8.4	3634727	G	A	seq	*srx-41*	G	A	A
	~+2.59	10552391	C	T	seq	*F32G8.2*	C	T	T
	+10.11	16472800	C	A	seq	*srw-35*	C	A	A
	+12.91	17454549	C	T	XbaI gain	*srh-203*	638 bps	217 + 421 bps	217 + 421 bps
X	-17.04	2119326	C	T	AccI loss	*gpa-5*	328 + 612 bps	940 bps	328 + 612 bps
	+1.73	9948218	C	T	seq	*nas-37*	C	T	T
	~+23.00	15844008	T	C	seq	*F59F4.3*	T	C	T

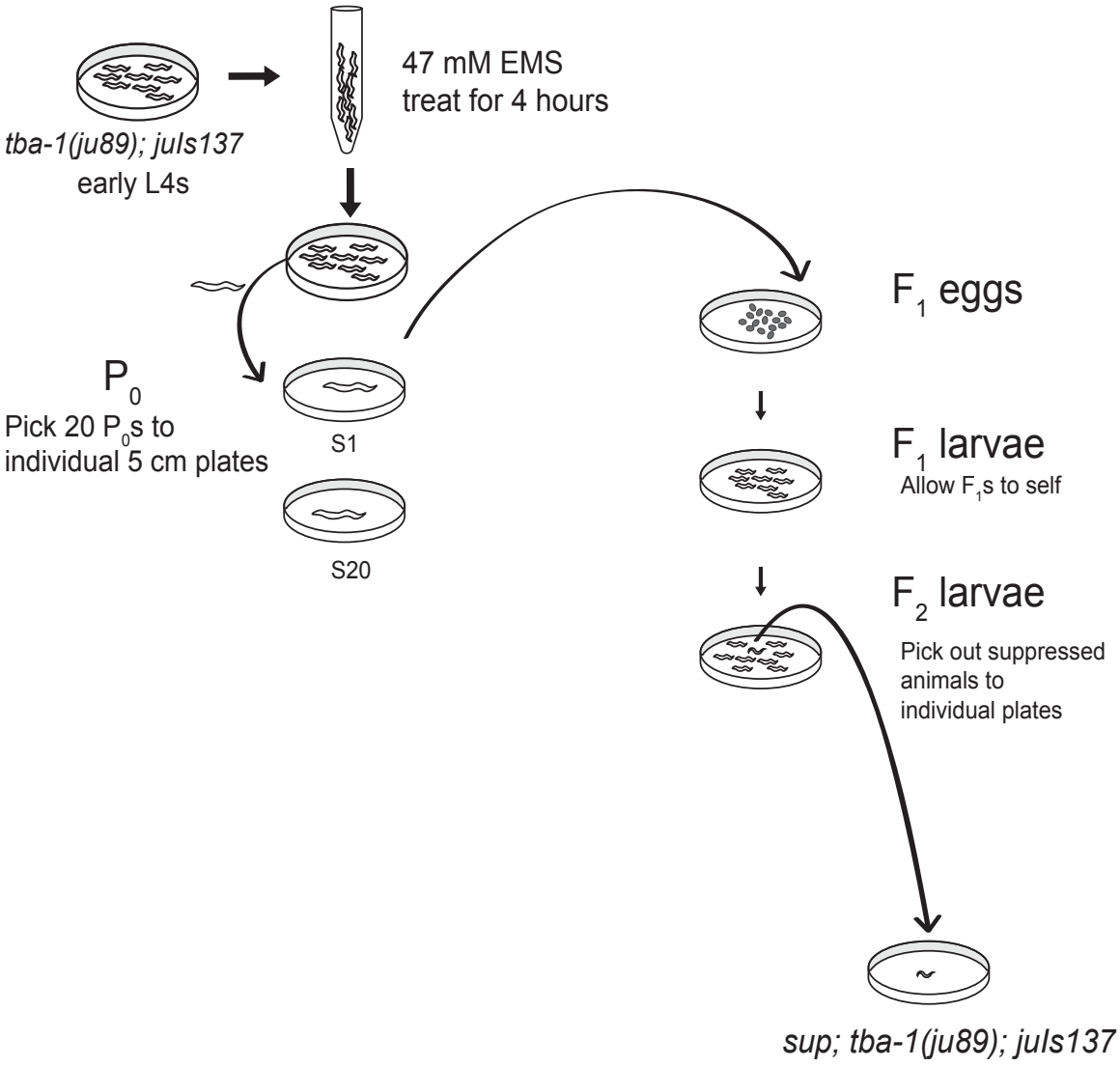

Figure 2.1 Suppressor screen in tba-1(ju89)

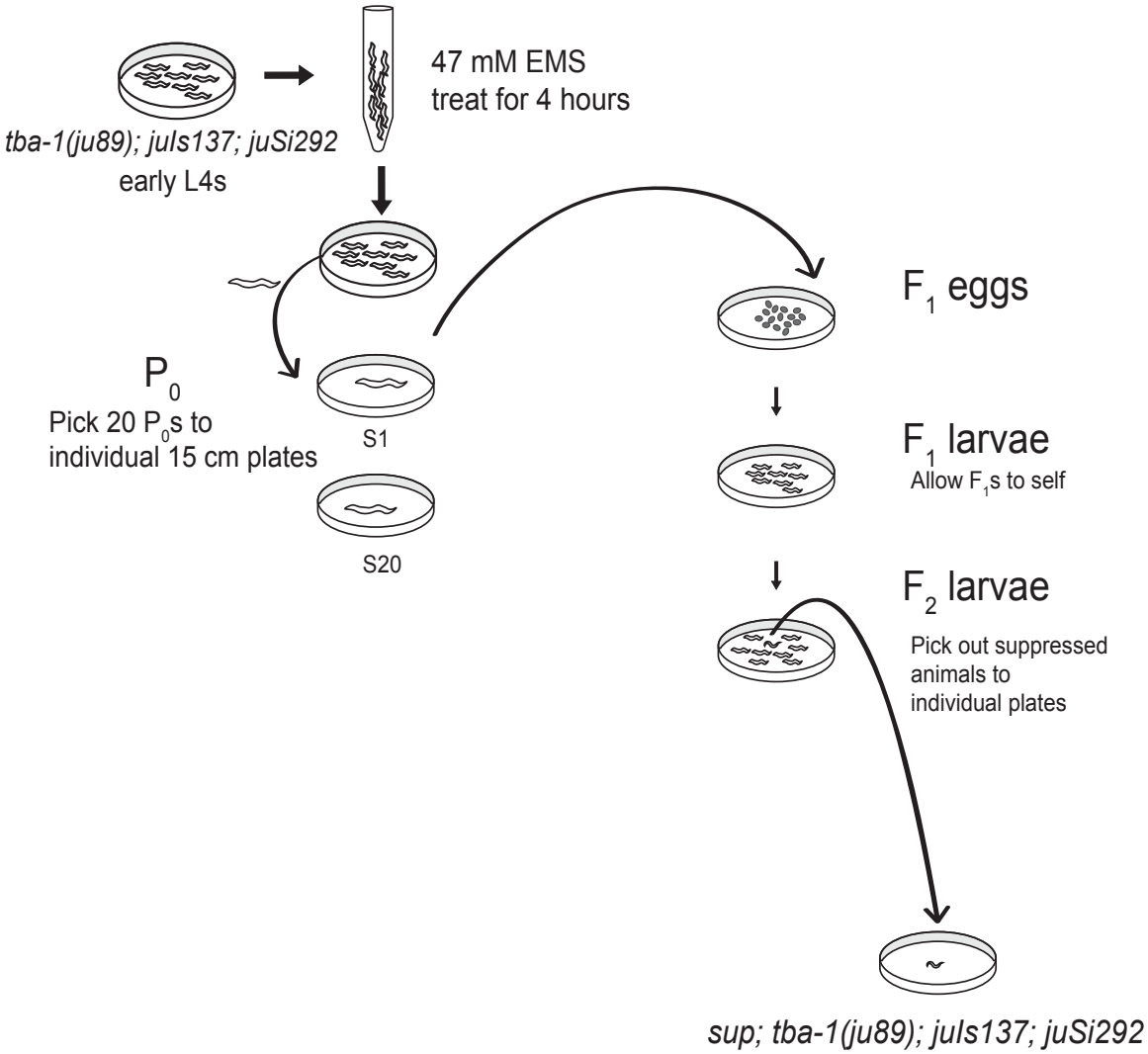

Figure 2.2: Suppressor screen in tba-1(ju89); juSi292

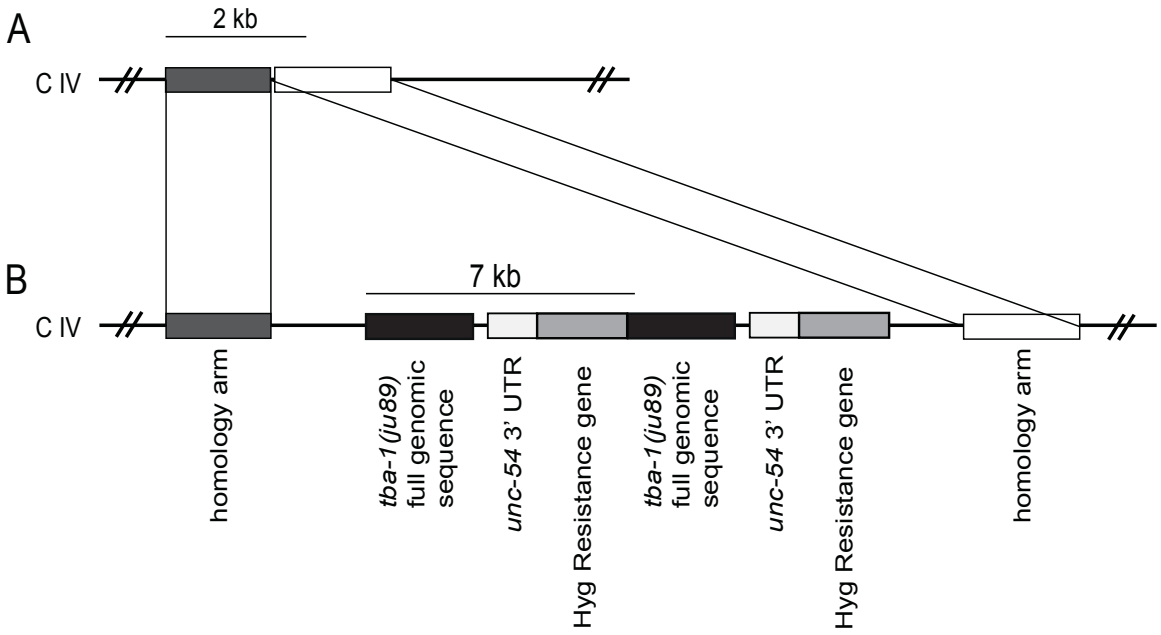

Figure 2.3: juSi292* is a double-copy insertion of *tba-1(ju89) I **A** Chromosome IV with homology arms used for insertion shown as rectangles. **B** Chromosome IV carrying *juSi292* insertion. 7 kb construct inserted twice in tandem.

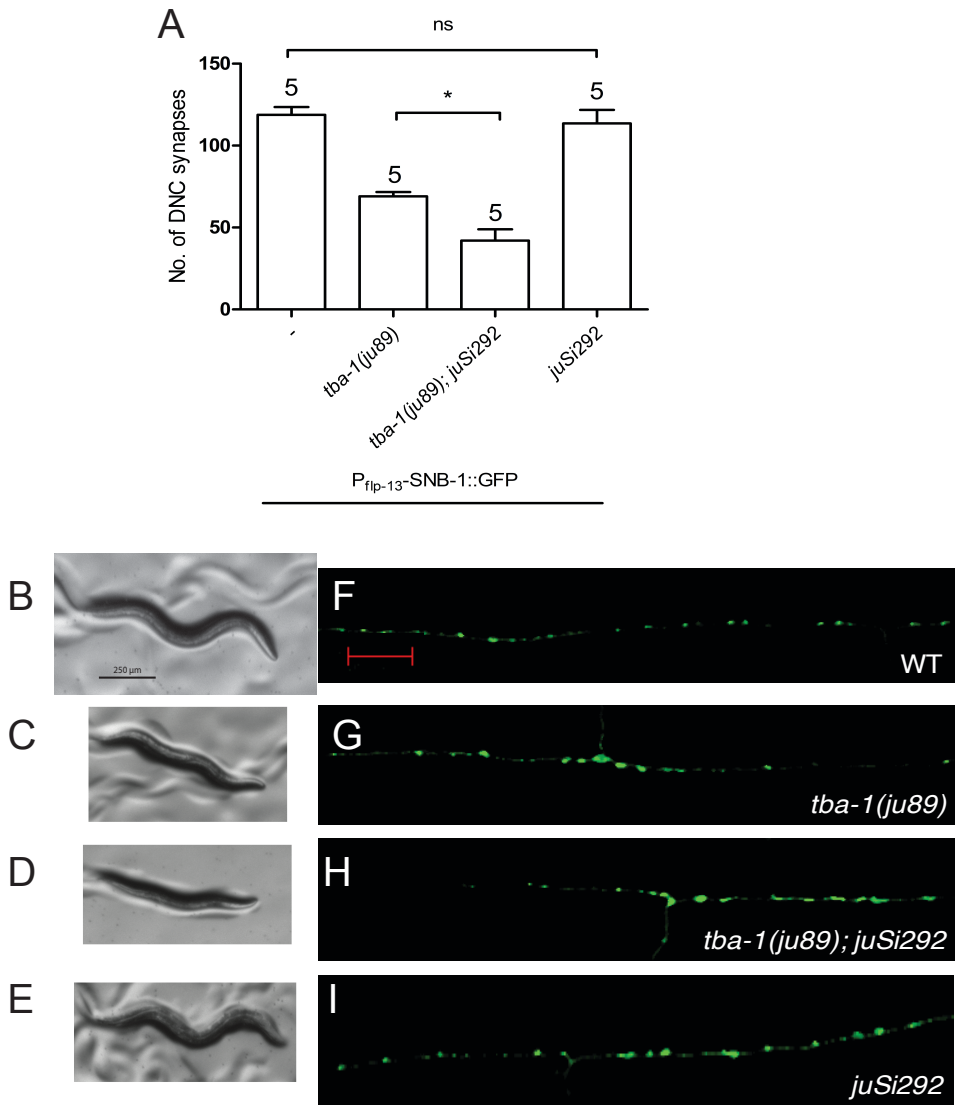

Figure 2.4 Characterization of juSi292 **I A** Number of dorsal nerve cord synapses in relevant genetic background. Number of animals screened (n) plotted above corresponding bar. Error bars represent SEM. **B-E** Images showing behavior for wild-type (B), *tba-1(ju89)* (C), *tba-1(ju89); juSi292* (D), and *juSi292* (E). **F-I** Representative images of synapses in DD neurons visualized using P_{flp-13}-SNB-1::GFP. Scale bar (F, red) represents 10 µm.

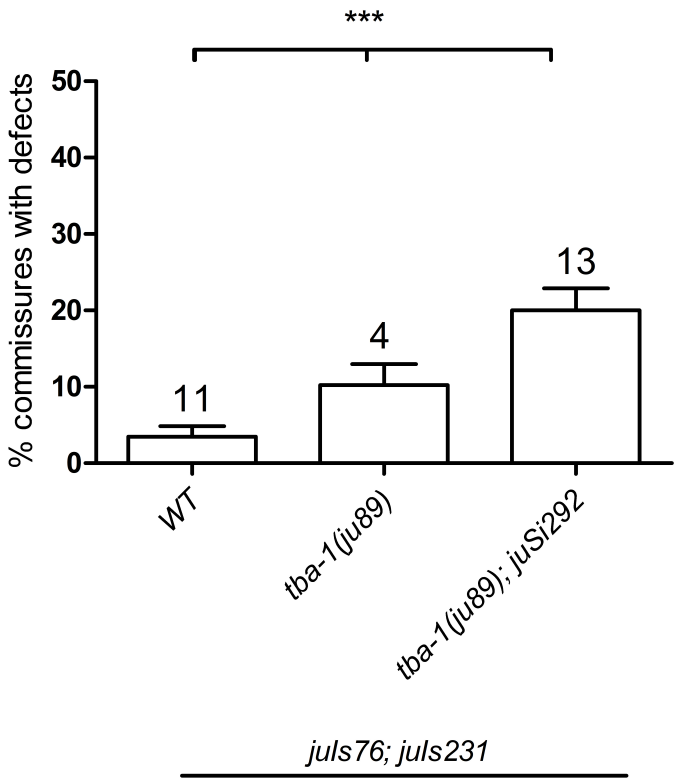

Figure 2.5: juSi292 increases commissural defects **I** Percentage of abnormal commissures counted per animal. Number of animals scored (n) plotted above corresponding bar.

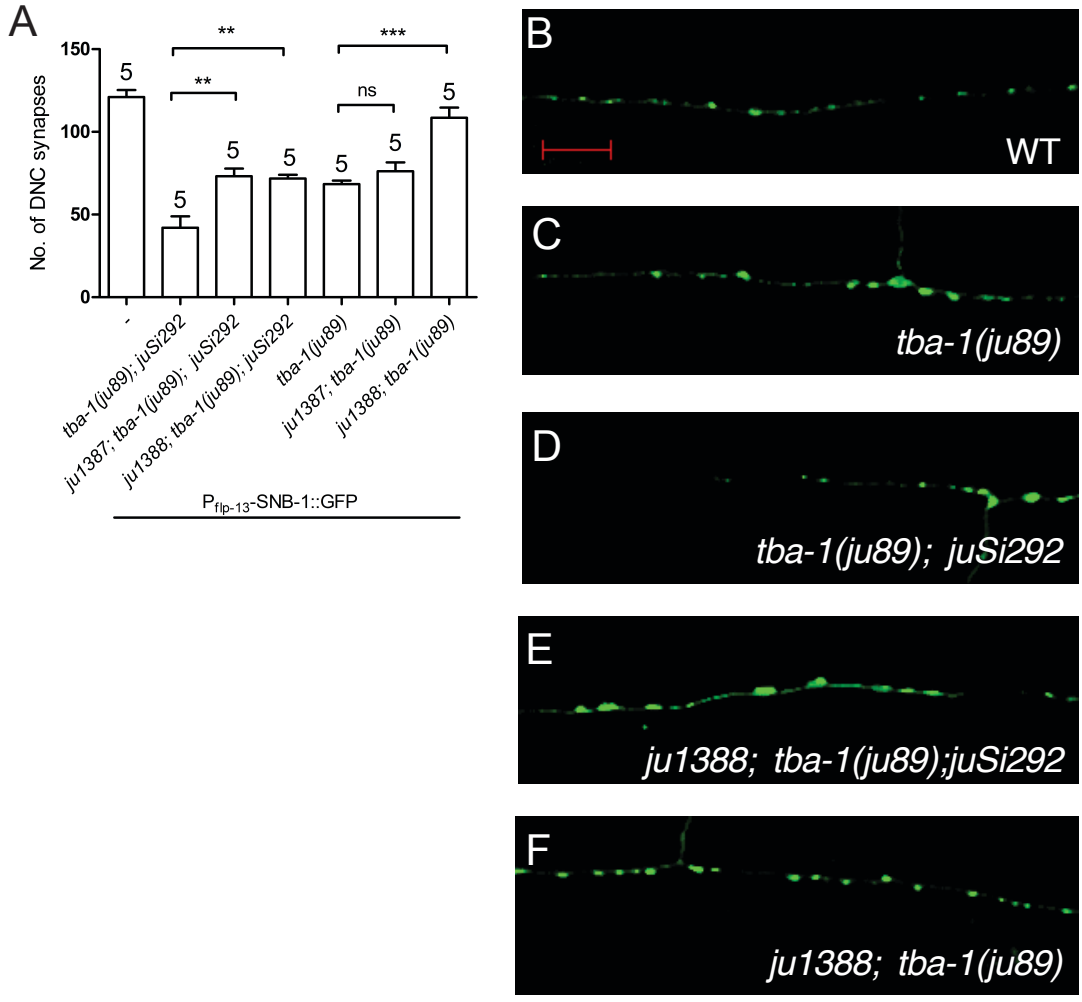

Figure 2.6: ju1388 strongly suppresses tba-1(ju89) **I A** Number of dorsal nerve cord synapses counted along dorsal nerve cord for relevant strains. Number of animals scored (n) plotted above corresponding bar. Error bars represent SEM. **B-F** Representative images of dorsal nerve cord synapses visualized using P_{flp-13}-SNB-1::GFP. Scale bar (red) is 10 µm.

REFERENCES

Baird, F. J., & Bennett, C. L. (2013). Microtubule defects & Neurodegeneration. *Journal of Genetic Syndrome & Gene Therapy*, *4*, 203. https://doi.org/10.4172/2157-7412.1000203

Baran, R., Castelblanco, L., Tang, G., Shapiro, I., Goncharov, A., & Jin, Y. (2010). Motor neuron synapse and axon defects in a C. elegans alpha-tubulin mutant. *PLoS ONE*, *5*(3). https://doi.org/10.1371/journal.pone.0009655

Baumbach, J., Murthy, A., McClintock, M. A., Dix, C. I., Zalyte, R., Hoang, H. T., & Bullock, S. L. (2017). Lissencephaly-1 is a context-dependent regulator of the human dynein complex. *eLife*, *6*, 1–31. https://doi.org/10.7554/eLife.21768

Brenner, S. (1974). Caenorhabdztzs elegans, 71–94.

Cartelli, D., & Cappelletti, G. (2016). Microtubule Destabilization Paves the Way to Parkinson???s Disease. *Molecular Neurobiology*, 1–13. https://doi.org/10.1007/s12035-016-0188-5

Chakraborti, S., Natarajan, K., Curiel, J., Janke, C., & Liu, J. (2016). The emerging role of the tubulin code: From the tubulin molecule to neuronal function and disease. *Cytoskeleton*, *73*(10), 521–550. https://doi.org/10.1002/cm.21290

Conde, C., & Cáceres, A. (2009). Microtubule assembly, organization and dynamics in axons and dendrites. *Nature Reviews Neuroscience*, *10*(5), 319–332. https://doi.org/10.1038/nrn2631
Gordon-weeks, P. R. (2003). Microtubules and Growth Cone Function, (March), 70–83. https://doi.org/10.1002/neu.10266

Hartman, J. J., & Vale, R. D. (1999). Microtubule Disassembly by ATP-Dependent Oligomerization of the AAA Enzyme Katanin, *286*(October), 782–786.

Horesh, D., Sapir, T., Francis, F., Wolf, S. G., Caspi, M., Elbaum, M., … Reiner, O. (1999). Doublecortin , a stabilizer of microtubules, *8*(9), 1599–1610.

Kurup, N., Yan, D., Goncharov, A., & Jin, Y. (2015). Dynamic Microtubules Drive

Circuit Rewiring in the Absence of Neurite Remodeling. *Current Biology*, *25*(12), 1594–1605. https://doi.org/10.1016/j.cub.2015.04.061

Kurup, N., Yan, D., Kono, K., & Jin, Y. (2017). Differential regulation of polarized synaptic vesicle trafficking and synapse stability in neural circuit rewiring in Caenorhabditis elegans, 1–20. https://doi.org/10.1371/journal.pgen.1006844

Molodtsov, M. I., Mieck, C., Dobbelaere, J., Dammermann, A., Westermann, S., & Vaziri, A. (2016). A Force-Induced Directional Switch of a Molecular Motor Enables Parallel Microtubule Bundle Formation. *Cell*, *167*(2), 539–552.e14. https://doi.org/10.1016/j.cell.2016.09.029

Munro, S. (2017). The Golgin Coiled-Coil Proteins of the Golgi Apparatus.

Pellegrini, L., Wetzel, A., Grannó, S., Heaton, G., & Harvey, K. (2017). Back to the tubule: microtubule dynamics in Parkinson's disease. *Cellular and Molecular Life Sciences*, *74*(3), 409–434. https://doi.org/10.1007/s00018-016-2351-6

Petersen, S. C., Watson, J. D., Richmond, J. E., Sarov, M., Walthall, W. W., & Iii, D. M. M. (2011). A Transcriptional Program Promotes Remodeling of GABAergic Synapses in Caenorhabditis elegans, *31*(43), 15362–15375. https://doi.org/10.1523/JNEUROSCI.3181-11.2011

Roos, J., Hummel, T., Ng, N., Klämbt, C., & Davis, G. W. (2000). Drosophila Futsch Regulates Synaptic Microtubule Organization and Is Necessary for Synaptic Growth. *Neuron*, *26*(2), 371–382. https://doi.org/10.1016/S0896-6273(00)81170-8

Ruiz-canada, C., Ashley, J., Moeckel-cole, S., Drier, E., Yin, J., & Budnik, V. (2004). New Synaptic Bouton Formation Is Disrupted by Misregulation of Microtubule Stability in aPKC Mutants, *42*, 567–580.

Wang, X., Shaw, W. R., Tsang, H. T. H., Reid, E., & Kane, C. J. O. (2007). Drosophila spichthyin inhibits BMP signaling and regulates synaptic growth and axonal microtubules, *10*(2), 177–185. https://doi.org/10.1038/nn1841

WHITE, J. G., ALBERTSON, D. G., & ANNESS, M. A. R. (1978). Connectivity changes in a class of motoneurone during the development of a nematode. *Nature*, *271*(5647), 764–766. Retrieved from http://dx.doi.org/10.1038/271764a0